Preclinical Assessment of a Zwitterionic Tantalum Oxide Nanoparticle X-ray Contrast Agent

Peter J. Bonitatibus, Jr.,* Andrew S. Torres, Binil Kandapallil, Brian D. Lee, Greg D. Goddard, Robert E. Colborn, and Michael E. Marino

GE Global Research Center, One Research Circle, Niskayuna, New York 12309, United States

ABSTRACT Tantalum oxide nanoparticles show great potential as the next generation of X-ray contrast media. Recently, we reported advances in tantalum oxide nanoparticles and identified improvements that were required for such particles to progress further. Namely, the viscosity of concentrated particles, the amount of retention in reticuloendothelial (RES) tissues, and the effect of large quantities of particles on the kidneys after administration were all identified as critical factors which needed further study, understanding, and development. Here, we report on a zwitterionic siloxane polymer nanoparticle coating that reduced the viscosity of concentrated solutions of particles by a factor of 5, decreased tissue retention of injected particles by a factor of 10, and, importantly, did not induce pathological responses in the kidneys.

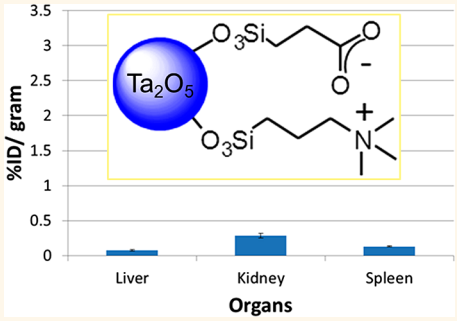

KEYWORDS: tantalum oxide · nanoparticle · X-ray contrast · zwitterion

Current X-ray contrast media consist of tri-iodobenzene derivatives that are exceptionally safe, in large part because compounds and formulations have been refined over the 60 years since their launch in order to continuously improve safety.[1] In contrast, pharmaceutical nanoparticles are only beginning to be understood. The result is that clinically viable nanoparticle X-ray contrast media will be evaluated against a very high safety standard that will require significant advancement in our understanding of the physicochemical features of nanoparticles that relate to biological performance.

We recently reported the tolerability, biodistribution, and physiologic response after application of such an approach using diethylphosphatoethyl-derivatized siloxane coated tantalum oxide nanoparticles (PHS-TaO) by administration to rats—initially at a dose of 400 mg tantalum/kg body weight with no physiological effects, and then at 1500 mg tantalum/kg body weight with minimal effects.[2] We identified critical factors that would hinder PHS-TaO from further progress as an X-ray contrast agent: namely, high viscosity upon agent concentration, retention in key organs, and an observable pathological response in the kidneys. The kidney response appeared to include inhibition of autophagy, a nanoparticle activity previously observed by others.[3−5] Although PHS-TaO was size-fractionated to increase the chance of renal clearance as 2−3 nm particles, it still accumulated significantly in the kidney as well as in the liver. It was hypothesized that making a more hydrophilic sub-5 nm particle would reduce the opportunity for protein binding and thereby reduce organ retention to desired levels (below 1.5% injected dose, % ID) in the entire animal within 48 h post-injection. We investigated PEG-derivatized siloxane-coated tantalum oxide nanoparticles (employing 2-[methoxy(polyethyleneoxy)-propyl] trimethoxysilane as a ligand); however, concentrated solutions (>250 mg Ta/mL) exhibited very high viscosities.[6]

In this report, we provide a preclinical assessment of newly developed zwitterionic siloxane polymer coated tantalum oxide nanoparticles (ZMS-TaO, see Scheme 1). This modification to a more hydrophilic coating decreased tissue retention of injected particles by a factor of 10, reduced the viscosity of concentrated solutions of nanoparticles by a factor of 5, and importantly, did not induce a pathological response in the kidneys, relative to what was observed for PHS-TaO nanoparticles. The novel zwitterionic siloxane polymer coating is considered an *intermolecular* zwitterion, in that two *different* organosilanes were used in equal amounts to ultimately generate a mixed charged siloxane polymer shell

* Address correspondence to bonitati@ge.com.

Received for review March 1, 2012 and accepted July 7, 2012.

Published online July 09, 2012
10.1021/nn300928g

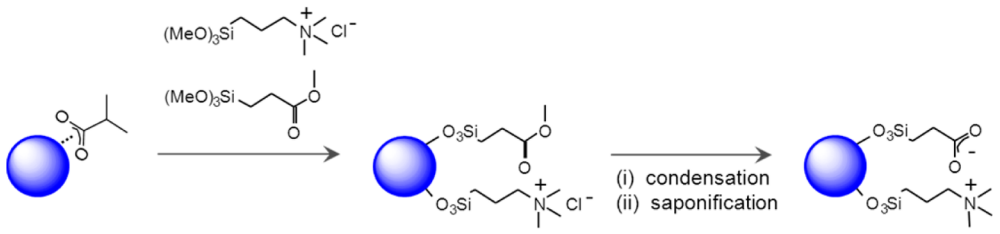

Scheme 1. Synthetic scheme to intermolecular zwitterionic polymer-coated tantalum oxide nanoparticles (ZMS-TaO). The blue circle symbolizes a tantalum oxide core and "O_3Si" is a simplification of the siloxane bonding structure.

on tantalum oxide. Silane-functionalized positively charged arms of the polymer were quaternary alkyl ammonium in nature (*i.e.*, propyl-*N,N,N*-trimethylammonium) and silane-functionalized negatively charged groups were carboxylates (*i.e.*, carboxyethyl) (Scheme 1). Although two different input organosilanes were employed to engender the formation of a zwitterionic siloxane polymer, the atom bearing either a positive or negative charge in the polymer arm was maintained at the fourth atom away from the silicon atom to minimize radial charge distribution.

We first disclosed this novel method of nanoparticle surface functionalization in several United States patent applications (2010) due to its ability to easily and robustly stabilize nanoparticles in physiological solutions,[7] and in 2011 Ji and co-workers reported a similar strategy of using mixed charged self-assembled monolayers (SAMs) to stabilize large gold nanoparticles.[8] Ji *et al*. mixed thioalkylated molecules, terminated with negatively and positively charged groups, in a 1:1 ratio to stabilize large gold nanoparticle dispersions in a wide pH range, in biological media, and at high salt concentration. Indeed, there have been reports of Au,[9−13] quantum dot,[14−17] and Ag[18,19] nanoparticles functionalized with thioalkylated zwitterionic small molecules; however, these other reports utilized *intramolecular* zwitterionic species bearing both a positive and negative charge in the same molecule.

To our knowledge, there are very few reports of polymeric (siloxane) zwitterionic nanoparticle coatings,[20−22] none of which utilize our mixed organosilane strategy. As such, herein we report our strategy of mixed organosilanes that form a zwitterionic siloxane polymer coating on the surface of tantalum oxide nanoparticles and provide our preclinical assessment of the X-ray agent.

RESULTS AND DISCUSSION

Nanoparticle Synthesis. We have discussed a modular system for the preparation of nanosized tantalum oxide cores, followed by *in situ* capping with desired shell materials, in previous reports.[2,7,23] In our standard conditions, a trialkoxy organosilane is added to cores transiently stabilized by isobutyric acid in alcoholic solvent (see Experimental Section). Concomitant with silane hydrolysis, surface attachment and condensation occur to form a siloxane polymer coating on tantalum oxide. In this report we employ two *different* organosilanes, used in equal amounts, to ultimately generate ZMS-TaO—a mixed charged zwitterionic siloxane polymer shell on tantalum oxide.

Outlined in Scheme 1 is our method using positively charged 3-(trimethoxysilyl)propyl-*N,N,N*-trimethylammonium chloride in combination with *the precursor to* a negatively charged silane, namely 2-(carbomethoxy)-ethyltrimethoxysilane. Using the carbomethoxy ester as a latent acid functionality allowed for ease of nanoparticle synthesis given its solubility in methanol. Both silanes are commercially available which enabled large scale synthesis (up to 0.5 kg Ta scale) at relatively low cost. As shown in Scheme 1, silane condensation and base hydrolysis of the carbomethoxy ester (to anionic carboxyethyl) are required to form the zwitterionic polymer coating. Although two different input organosilanes were employed, the atom bearing either a positive or negative charge in the polymer arm was the fourth atom away from the silicon atom to minimize radial charge distribution. Since both input organosilanes are trimethoxysilanes, addition of a combined silane mixture that used equal moles of each silane and tantalum minimized preferential attachment of one silane over another considering hydrolysis and condensation rates are comparable. In fact, the relative ratio of silane-functionalized positively charged groups to negatively charged groups on the polymer was close to 1:1 based on characterization data acquired using fractionated purified material (*vide infra*).

Structure and Purity. The zwitterionic siloxane polymer provided distinctive signatures in NMR spectra to characterize it as a nanoparticle coating. ^{1}H NMR spectral resonances in D_2O are broadened significantly, indicative of (1) surface attachment due to slow tumbling nanoparticles, therefore ligand protons undergo fast T2 relaxation, and (2) a subtle magnetic inhomogeneity between otherwise equivalent ligand protons, due to the ligand−nanoparticle surface bonding structure (*i.e.*, spin−lattice relaxation, T1). Assignments for the ^{1}H spectrum in Figure 1 are as follows: 3.32 ppm (CH_2 close to $^+N(CH_3)_3$), 3.11 ppm ($^+N(CH_3)_3$ protons), 2.36−2.25 ppm (CH_2 close to carboxyl), 1.90 (middle CH_2 of $^+N(CH_3)_3$ ligand), 0.83 ppm (CH_2

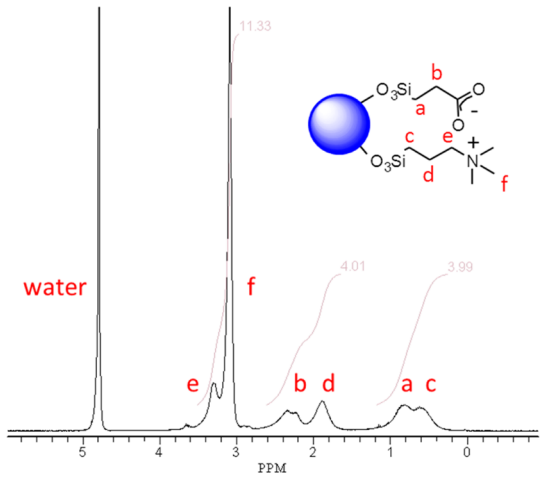

Figure 1. ^{1}H NMR spectrum of ZMS-TaO. The blue circle symbolizes a tantalum oxide core and "O_3Si" is a simple representation of the siloxane polymer structure. Protons a–f of the coating are assigned as noted.

close to Si of carboxyl ligand), 0.60 ppm (CH_2 next to Si of $^{+}N(CH_3)_3$ ligand). Aside from the broadening, resonances are not significantly different or shifted when compared to spectra of hydrolyzed input organosilanes. The shifts are slightly downfield by ~0.03 ppm. Noticeably *absent* from the ^{1}H spectrum are the methoxy protons from the starting trimethoxysilane groups and signals from isobutyric acid. Treatment of particles with HCl and subsequent tangential flow filtration (TFF) washing of the particles with NaCl are sufficient steps to remove traces of methanol, ethanol, and isobutyric acid (see Experimental Section). Of particular note are the comparable intensities and integrated ratios of the two peaks between 0.5 and 1 ppm, which are methylene resonances from the carbons adjacent to Si on each charged arm of the polymer. The peak at 0.83 ppm belongs to the Si–CH_2 of carboxylate ligand, and the more upfield peak at 0.60 ppm is assigned to the quaternary alkyl ammonium Si–CH_2 group.

From ^{29}Si NMR spectroscopy, it is clear that trimethoxysilane ligands underwent hydrolysis and a high degree of condensation to form a siloxane coating on the nanoparticle surface. The ^{29}Si spectrum (see Supporting Information, Figure S1) featured two broad peaks between −50 and −70 ppm, which is indicative of Si atoms with 2 and 3 O–Si groups attached as R*Si*$(OSi)_2$ and R*Si*$(OSi)_3$, respectively (or T^2 and T^3 structures). ^{29}Si spectra of freshly prepared and 1 month aged concentrated samples (~150 mg Ta/mL) were not significantly different, suggesting the siloxane coating remained intact and is fairly stable over this period of time. It should be noted that at roughly *30-fold dilution* of the as-synthesized sample, a second set of tiny sharp resonances were observed superimposed on the corresponding set of broad peaks in the ^{1}H spectrum. The sharp peaks proved to be the hydrolyzed trisilanol analogues of the siloxane coating existing up to 2% of each free ligand in solution (*vide infra*). The most interesting feature in the ^{29}Si spectrum is the signal between −44 and −49 ppm. According to a study of inorganic/organic hybrid materials containing glycidoxypropyltrimethoxysilane and tantalum ethoxide, the signal for Si–O–Ta appeared from −47 to −49 ppm in the ^{29}Si spectrum.[24] Although characterization of the exact bonding structure between the particle surface and the siloxane coating is unknown, the peak observed between −44 and −49 ppm in our ^{29}Si NMR spectrum served as evidence for Si–O–Ta bonding. Taken together, ^{29}Si NMR data supports a high degree of organosilane condensation and association to the tantalum oxide surface.

From the literature, an infrared (IR) band at 947 cm^{-1} was assigned to the Si–O–Ta bond in Ta_2O_5/SiO_2 mixed nanoparticles.[25] However, the IR spectrum for our system in that region showed only strong Si–O–Si vibrational modes as overlapping intense bands between 1015 and 925 cm^{-1}, characteristic of siloxane layers (see Supporting Information, Figure S2). Likewise, it was impossible to determine the presence or absence of Ta═O because Si–O–Si vibrations obscure the region at 975 cm^{-1}. Other noteworthy features observed in the IR were the quaternary ammonium (3365–3200 cm^{-1}) and the deprotonated carboxyl group. Vibrational modes of the carbonyl oxygen, and coupling to the second oxygen atom, were clearly visible at 1653 and 1559 cm^{-1}, respectively.

Structural characterization data for ZMS-TaO also included nanoparticle size by DLS and element compositional analysis by ICP–AES. Mean particle diameter of material purified as a 50–5 kDa fraction (see Experimental Section) measured 5 nm, although volume-weighted distribution functions from batches of nanoparticles revealed a bimodal size distribution, with a population of 1.5–2.5 nm and another between 4 and 6 nm. The intensity-weighted distribution function is included as Supporting Information, along with a representative TEM micrograph of the nanoparticles. ZMS-TaO particle size remained unchanged after formulation with phosphate-buffered saline using amounts appropriate to achieve a solution iso-osmolar with blood. ICP–AES was used directly to quantitatively determine both Ta and Si mg/g-aqueous-sample, and this data was used to then calculate a Si/Ta mole ratio of 1.51. It is worth noting, a Si/Ta mole ratio of 2 was used in the synthetic process to ensure complete surface coverage by input organosilanes. ICP–AES data also allowed for calculation of yield, as ~84% based on mass elemental tantalum charged, and weight percent tantalum as freeze-dried purified ZMS-TaO nanoparticles (41% by weight tantalum).

In addition to ^{1}H NMR, purity was assessed by methods including hyphenated techniques and conductivity. In a previous report, we discussed chromatographic analysis of nanoparticles by HPLC using

ICP–AES detection.[23] Here again for ZMS-TaO, tantalum and silicon emission spectra were observed as coeluting LC peaks to indicate a single species and nanoparticle homogeneity. Regarding HPLC-ICP, a shortcoming of this technique is an inability to detect *low-level* excess Si-containing material (*i.e.*, trisilanol) that is not attached to the nanoparticle surface, but ion-paired to the siloxane polymer and carried through HPLC–ICP analysis. In an attempt to quantify low-level "free" trisilanol (a result of siloxane hydrolysis at very dilute tantalum concentration, *vide supra*), we employed a flow injection analysis in combination with time-of-flight mass spectrometry (ToF-MS). Dilute nanoparticle solutions were injected directly into the electrospray ionization (ESI) chamber, with the presumption that large nanoparticles (2–5 nm) would not ionize and would fall out of the desolvation stream, to exclusively ionize and detect free trisilanol in solution. In the case of analyzing for free quaternary ammonium trisilanol, quantification was facilitated by (1) the ionization efficiency of a quaternary ammonium functional group, and (2) the fact that 3-(trimethoxysilyl)propyl-*N,N,N*-trimethylammonium-^{15}N chloride was commercially available at a reasonable cost. Supporting Information, Figure S3 includes a spectrum to show that response and resolution were more than adequate to quantify low-levels of free quaternary ammonium trisilanol against the ^{15}N internal standard. Supporting Information, Figure S4 shows a calibration curve over the range of 0–80 μg/mL for free quaternary ammonium trisilanol to demonstrate good linearity and reproducibility in this dynamic range. With this data, it was possible to determine that at a significantly dilute concentration (roughly 5 mg Ta/mL) approximately 2% of the total quaternary alkyl ammonium in the system existed as free quaternary ammonium trisilanol.

The conductivity of purified nanoparticle solutions was measured to check for unwanted residual ions leftover from synthesis and processing. Typically, conductivities for purified material ranged between 100 and 200 μS over a concentration range of 25–35 mg Ta/mL. The highest conductivity measured for a purified batch of 5 kDa retentate was 223 μS at 30 mg Ta/mL.

While it is rather difficult to quantify the exact ratio of silane-functionalized positively charged groups to negatively charged groups on one nanoparticle, we can qualitatively confirm that the two groups are present in comparable amounts from ^{1}H NMR peak integration (*vide supra*) and overall surface charge (zeta potential) measurements. The zeta potentials of particles were determined as a function of pH to generate an isoelectric point (IEP) titration curve and assess surface charge response across a pH range. At low pH in 8.5 mM ammonium bicarbonate buffered solution, the zeta potential of ZMS-TaO was positive which is consistent with amine and protonated carboxyl groups imparting a positive charge to the particle surface (Supporting Information, Figure S5). At neutral pH the zeta potential was negative (−12 mV). In fact, a shift to *slightly* negative zeta potential was observed at all pH values above the observed isoelectric point of 4.3. The data and associated charge response is consistent with zwitterionic character in that at low pH the zeta potential is positive, while at higher pH the zeta potential measurements shifted negative.[22] In addition to ammonium bicarbonate buffer, zeta potential measurements were recorded in different salt environments. Using hydroxide ion to adjust salt media to neutral pH (near pH 7.4), the zeta potential of ZMS-TaO in 15 mM NaCl was observed as −8 mV. To approximate the Na/Ca ratio found in blood, a solution of 15 mM NaCl and 2 mM $CaCl_2$ was utilized in which ZMS-TaO measured −1.5 mV. Despite the dependency of zeta potential measurements on a chemical (salt) environment, we conclude from this data that ZMS-TaO is near charge-neutral under *in vivo* conditions considering the measured overall very low negative zeta potential values.

Physicochemical Parameters. Clinically speaking, iodinated X-ray contrast agents are administered in concentrations of approximately 200–400 mg **I**/mL injected solution. Such highly concentrated solution doses are required to generate sufficient X-ray contrast in reasonably injectable volumes. The physicochemical properties of solutions at these concentrations, including viscosity and osmolality, have an impact on X-ray agent practical usage. High viscosity can prevent administration through a catheter and also impact patient safety.[26] Hyperosmolality has been linked to reduced patient comfort and increased risk of side effects.[27] Therefore, improving physicochemical properties of tantalum oxide *nanoparticle solutions* are critical to their viability as X-ray contrast media and must be considered during preclinical assessment.

Previously, we reported that the practical viscosity limit of 25 cps was reached at 190 mg Ta/mL (37 °C) with fractionated 2–3 nm diethylphosphatoethylsiloxane-coated tantalum oxide agent PHS-TaO.[2,23] This agent was deemed untenable at potentially *clinically relevant* concentrations (≥250 mg Ta/mL) due to viscosity limitations. At solution viscosities above 25 cps, standard injection rates of >4 mL/sec are not feasible due to back pressure generated when pushing viscous materials through a catheter and vasculature.[28] In this work, we developed similarly sized and purified nanoparticles featuring a zwitterionic siloxane polymer coating that demonstrated reduced viscosities, relative to PHS-TaO, at all concentrations and achieved the viscosity target (<25 cps) in a *clinically relevant* concentration range. As can be seen in Figure 2, the viscosity of ZMS-TaO correlates with tantalum concentration and starts to increase exponentially above 200 mg Ta/mL. Only at around 275 mg Ta/mL did the viscosity reach a value of approximately 20 cps. For comparison with ZMS-TaO, viscosity measurements of

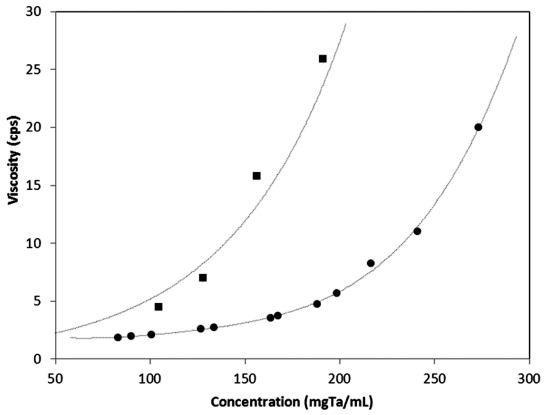

Figure 2. Viscosity data measured at 37 °C for ZMS-TaO (circles) and PHS-TaO (squares) nanoparticles, with calculated fits (lines) to plotted experimental data.

PHS-TaO are included in Figure 2. It is clear at 190 mg Ta/mL, the viscosity of ZMS-TaO has been reduced by a factor of 5 relative to PHS-TaO. In terms of osmolality, solutions of ZMS-TaO are similar to PHS-TaO in that solutions at 200 mg Ta/mL are hypo-osmolar (200 mOsm/kg) compared to blood (290 mOsm/kg). Indeed, these nanoparticle solutions were not hyperosmolar (>290 mOsm/kg) until a concentration greater than 275 mg Ta/mL was reached (Supporting Information, Figure S6).

Agent Preparation. The choice of formulation and the level of purity of a compound can have a dramatic impact on its effects in an animal model. For ZMS-TaO and PHS-TaO, extensive characterization (as shown above for ZMS-TaO) was carried out for each batch of material to ensure purity, and formulations were carefully controlled to ensure the relevance of all *in vivo* results. *In vivo* studies were performed using a standard concentration of agents at 150 mg Ta/mL to normalize dosing volume for different agents. At this concentration, ZMS-TaO and PHS-TaO agents were hypo-osmolar to blood. To address hypo-osmolality and minimize the possibility of formulation-dependent damage to blood cells, ZMS-TaO and PHS-TaO agents used for comparative *in vivo* studies were formulated to iso-osmolality (290 mOsm/kg) using concentrated phosphate-buffered saline (10× PBS). Agents were then tested for sterility to control for formulant-mediated contamination. Both ZMS-TaO and PHS-TaO agents used in these studies were negative for measurable endotoxin at a sensitivity of >5 EU/mL and our sterile handling techniques were sufficient to formulate agents without contamination. Regulatory standards indicate a maximum of 5 EU/kg/h for pharmaceuticals, which is within the range measured for ZMS-TaO in rats (max. dose 2.5 EU/kg). Using methods previously discussed,[2] we analyzed formulated ZMS-TaO for evidence of endotoxin contamination. Manufacturer protocols require spike recovery of a standard in order to validate measurements on agents. All attempts to measure ZMS-TaO at concentrations greater than 30 mg Ta/mL did not allow for spike recovery. It was therefore necessary to dilute formulated samples to 0.3 mg Ta/mL to measure endotoxin concentrations. Our studies with ZMS-TaO indicate some interference with the LAL-based endotoxin test method and further studies are in progress to address this finding. Recent reports have shown that nanomaterials interfere with commercially available LAL-based endotoxin tests.[29,30]

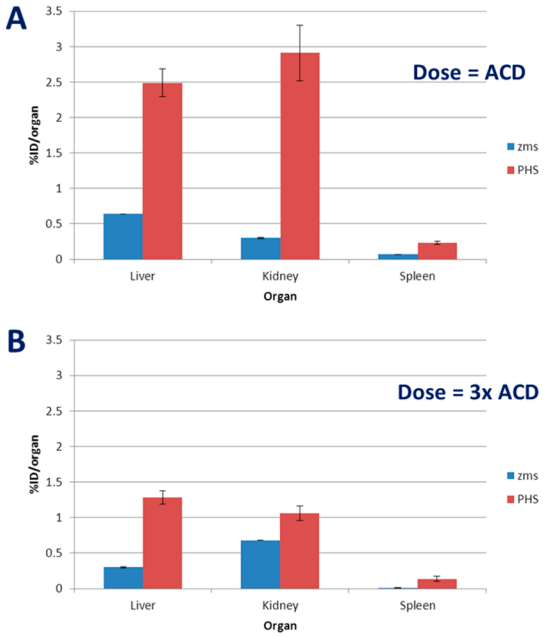

Figure 3. Tissue retention of ZMS-TaO versus PHS-TaO at 7 days postinjection in rats (n = 3 per cohort). (A) Retained Ta at ACD is lower for ZMS-TaO than for PHS-TaO, (B) Retained Ta at 3× ACD is lower for ZMS-TaO than for PHS-TaO.

Tissue Retention Studies. Low tissue retention and rapid clearance are important for minimizing safety risk. High levels of tissue exposure (the product of concentration and time) generally correlate with a higher likelihood of an adverse tissue response.[2,31] Given that the anticipated clinical dose (ACD) for these X-ray nanoparticle agents is high in comparison to agents used for all other contrast-enhanced imaging modalities, tissue retention was evaluated at ACD and at three times ACD. Naïve rats (n = 3 per cohort) were intravenously injected while awake with ZMS- and PHS-TaO *via* tail vein at both ACD for CT imaging (400 mg Ta/kg) and approximately three times this dose (1500 mg Ta/kg). Because both of these particle agents are between approximately 30 and 40% Ta by mass, this represents a molecular dose of injected particles of approximately 1−1.2 g and 4−4.5 g of particle/kg! We collected major clearance organ tissues (liver, kidney, and spleen) from injected animals at several key time points and evaluated clearance and retention of our agents over time.

We observed a significant decline in the retention of Ta using ZMS-TaO *versus* PHS-TaO (Figure 3). Kidney

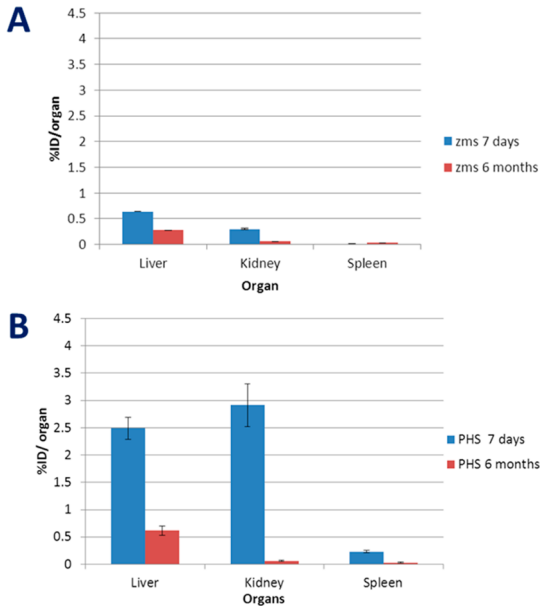

Figure 4. Tissue retention of ZMS-TaO *vs* PHS-TaO over time at ACD (400 mg Ta/kg) in rats (n = 3 per cohort). Retained Ta in liver and kidney shows gradual decline of retained material over time.

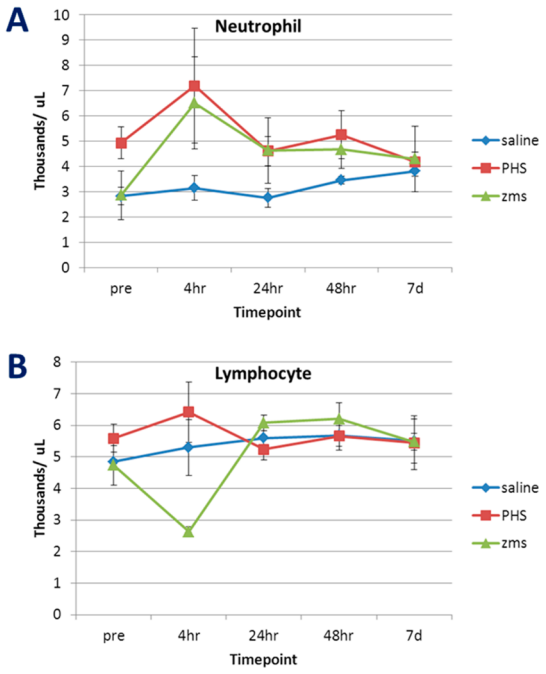

Figure 5. Complete blood count longitudinal analysis after ACD (400 mg Ta/kg) injection of tantalum oxide nanoparticle agents in rats (n = 4 per cohort). (A) Neutrophil counts showed similar trends after injection of ZMS-TaO and PHS-TaO. (B) Lymphocyte featured transient but dramatic decline immediately following injection of ZMS-TaO. All data are referenced against saline injected rats (n = 4).

retention in particular decreased by an order of magnitude, a rather significant finding given our recent report on the impact of retained agent on kidney pathology using PHS-TaO.[2] Histopathology of these tissues also demonstrated that at both ACD and approximately three times ACD, ZMS-TaO did not induce pathology such as that observed previously with PHS-TaO (Supporting Information, Figure S7). We hypothesize that efficient renal clearance enabled this improvement, based on the excretion data collected one day after injection of ZMS-TaO (Supporting Information, Figure S8). The bulk of the injected material was found in urine, with only a very limited amount (<3%) found remaining in the carcass (Figure S8). It is worth highlighting that the study also revealed a decrease in the percent of the agent retained as the dose increased from ACD to approximately three times ACD. This reduction may reflect a saturated uptake mechanism for nanoparticles, a possibility that can be further evaluated once such mechanisms are better understood.[2]

Zwitterionic coatings are known to decrease protein binding and provide a roughly neutral zeta potential to particles.[8−17,20−22,32−38] This feature of ZMS-TaO may enable the very efficient clearance kinetics observed, even at elevated doses. Iodine-based X-ray contrast agents, which are typically nonionic and demonstrate low protein binding, also have similar retention profiles in kidney.[39] This represents a tremendous step forward in designing Ta-based nanoparticles that can attain the biological performance required for clinically viable agents.

Despite rapid clearance and reduced tissue retention exhibited by ZMS-TaO, clearance of retained material was monitored for several months after injection (Figure 4). ZMS-TaO agent does in fact clear over time from liver and kidney, much like PHS-TaO. No pathological response was observed in these tissues (Supporting Information, Figure S7) and animals injected with ZMS-TaO did not demonstrate different growth rates or organ weights as compared to saline-injected control animals. Though the precise molecular mechanism for clearance of retained tantalum oxide nanoparticles is not known at this time, we report evidence that even modest levels of retained agent decreased over time without visible impact to tissue or tissue function (Supporting Information, Figures S7 and S9).

Tolerability Studies. Tolerability studies were performed to understand the acute and chronic impact of these agents in naïve rats. All injections were performed in restrained rats while the animals were awake in order to minimize interference of biological responses due to anesthetic.[40] Standard data collected for these studies include body and organ weights, clinical chemistry, and complete blood count. At an ACD of 400 mg Ta/kg and at approximately three times ACD (1500 mg Ta/kg), animals injected with ZMS-TaO did not show any observable acute or chronic effects over 7 days following injection. Animals gained weight at rates comparable to saline-injected animals and the weights of organs at necropsy were not significantly different between ZMS-TaO and saline-injected animals. Clinical chemistry analysis did not reveal impact

to organ function at either dose (Supporting Information, Figure S9). We did note that both ZMS-TaO and PHS-TaO demonstrated a spike in neutrophil numbers at 4 h, and that ZMS-TaO injected animals developed a transient decrease in lymphocyte count (by CBC) that was distinct from PHS-TaO, but all values returned to baseline within 24 h (Figure 5 and Supporting Information, Figure S10). It is possible that the lymphocyte depletion observed for ZMS-TaO injected animals is due to particle-mediated activation of the innate immune response; however, clarification of this mechanism was beyond the scope of the current study. Immunological impacts have been observed in other nanomaterials upon interaction with blood, though rats are known to be a poor model of this effect.[41−43]

CONCLUSION

A tremendous step forward in the design of nanoparticle-based X-ray contrast media has been made with development of ZMS-TaO. Preclinical assessment suggested physicochemical properties and biological performance met criteria required for clinically viable X-ray contrast agents. A more hydrophilic (zwitterionic) coating on tantalum oxide resulted in nanoparticles that achieved the viscosity target of <25 cps at 275 mg Ta/mL, and histopathological evaluation of kidney tissue demonstrated that at approximately three times ACD, ZMS-TaO did not induce pathology such as that observed with previous tantalum oxide agents (PHS-TaO). We hypothesize that highly efficient renal clearance enabled this improvement.

The growing understanding of the relationship between particle coating and its biological impact will shape future efforts. Tantalum oxide nanoparticles have tremendous promise as novel X-ray contrast media. Continued efforts to understand the physiologic impact of nanoparticles at very high dose will support further progress, and additional studies identifying novel applications for such an agent will justify it.

EXPERIMENTAL SECTION

Materials. Tantalum ethoxide ($Ta(OEt)_5$) was obtained from H. C. Starck as a 1 kg lot and used as received. Deionized water (18.2 MΩcm resistivity) was prepared with a Milli-Q Biocel Millipore filtration system, equipped with a QuantumEX Ultrapure Organex cartridge and 0.22 μm filter, and used for all aqueous sample dilutions and washings. The trimethoxy organosilanes, 2-(carbomethoxy)ethyltrimethoxysilane and 3-(trimethoxysilyl)propyl-*N,N,N*-trimethylammonium chloride, were purchased from Gelest, Inc. and used as received. Deuterium oxide was obtained from Cambridge Isotope Laboratories (99.9% deuterium) and used as received. Regenerated cellulose (RC, 5 kDa MWCO) and polyethersulfone (PES, 50 kDa MWCO) TFF membranes were obtained from Millipore. All other reagents and solvents were purchased from Aldrich or Fisher and used as received.

ZMS-TaO Synthesis. To 680 mL anhydrous methanol in a 2 L flask, was added 10 mL isobutyric acid and 2.78 mL deuterium oxide at room temperature under stirring in a nitrogen-filled glovebox. This mixture was stirred for 40 min after which tantalum ethoxide (37.36 g) was added in a dropwise manner (not quite a stream) over a period of 15−20 min. The hydrolysis reaction was allowed to stir for 5 h after which the flask was removed from the glovebox and placed under an inert atmosphere using a Schlenck-/vacuum-line manifold. After 5 h of hydrolysis, both trimethoxysilanes were added simultaneously. 2-(Carbomethoxy)ethyltrimethoxysilane (19.16 g) was combined with 3-(trimethoxysilyl)propyl-*N,N,N*-trimethylammonium chloride (47.44 g, sold as a ∼50% solution in methanol), and the mixture was added directly to the 2 L reaction vessel as quickly as possible. The mixture was then refluxed overnight under nitrogen. The next day, the reaction mixture was cooled to room temperature, and 6 mL of 0.15 M ammonium hydroxide was added dropwise while stirring. After 3 h, 60 mL of MQ water was added dropwise, and the reaction mixture was set to stir overnight at room temperature. Next, 360 mL of 0.67 M HCl was added dropwise under stirring, and the reaction was then heated to 50 °C for 5.5−6 h (pH 1−2). After the solution cooled to room temperature, the reaction was neutralized using 5.92 M ammonium hydroxide (dropwise) to achieve a pH between 7.5 and 8.

To hydrolyze the methyl ester, all volatiles were removed by rotary evaporation at 50 °C, and residual solids were treated, in the same 2 L vessel, with 250 mL of 5 M ammonium hydroxide solution. The resulting mixture was stoppered and stirred for 3 days at room temperature.

To end the hydrolysis, the reaction was brought to pH 8 using 3 M HCl. The batch was filtered through a 0.22 μm sterile filter, brought to a volume of 1 L with water, then processed through a polyethersulfone (PES) 50 kDa MWCO filter membrane (0.1 m^2) using tangential flow filtration (TFF). To maximize product recovery, 16 L of 0.5 M NaCl, followed by 4 L MQ water, were processed in the TFF apparatus and all permeate collected. Time required for this filtration was about 60 min. Final purification/fractionation used a regenerated cellulose (RC) 5 kDa MWCO membrane (0.2 m^2) and required 18 L of MQ water wash volume. Over the course of 24 h, all permeate was processed against the 5 kDa MWCO filter, along with the 18 L of water. The retentate in the reservoir was concentrated to approximately 700 mL and filtered through a 0.22 μm sterile filter. After fractionation, 9 mL of the 5 kDa retentate was removed for analysis: 1.5 mL for ICP−AES to determine both Si and Ta mg/g sample; 1 mL of freeze-dried for NMR; 4 mL for size by DLS at ∼30 mg Ta/mL, followed by conductivity testing; and the remainder for HPLC-ICP, pH, and endotoxin testing. The batch was then stored at 4 °C for further experiments. Upon completion of characterization, the material was concentrated by rotary evaporation at 40 °C and used for biological experimentation and more physicochemical characterization (*i.e.*, viscosity).

Characterization of ZMS-TaO as a 5 kDa retentate included elemental analysis by ICP−AES: 41.4% by weight tantalum as a freeze-dried solid and mol ratio Si/Ta of 1.51; yield of 83−85% based on elemental tantalum mass charged; DLS with a mean particle diameter of 5 nm, although volume-weighted distribution functions from batches of nanoparticles reveal a bimodal size distribution, with a population of 1.5−2.5 nm and another between 4 and 6 nm. Particle size remains unchanged after formulation with phosphate-buffered saline using amounts appropriate to achieve a solution iso-osmolar with blood. Conductivity: 100−200 μS over a concentration range of 25−35 mg Ta/mL. ^{1}H NMR (400 MHz, D_2O): 3.32 ppm (CH_2 close to $^+N(CH_3)_3$), 3.11 ppm ($^+N(CH_3)_3$ protons), 2.36−2.25 ppm (CH_2 close to carboxyl), 1.90 (middle CH_2 of $^+N(CH_3)_3$ ligand), 0.83 ppm (CH_2 close to Si of carboxyl ligand), 0.60 ppm (CH_2 next to Si of $^+N(CH_3)_3$ ligand). ^{29}Si NMR (600 MHz): −46 ppm (*Si*−O-Ta), −53 ppm (R(HO)*Si*$(OSi)_2$), −61 ppm (R*Si*$(OSi)_3$). IR (freeze-dried powder in mineral oil between NaCl plates): vibrational modes of the carbonyl oxygen, and its coupling to the second

oxygen atom, are clearly visible at 1653 and 1559 cm^{-1}, Si−O−Si vibrations 1015−925 cm^{-1}, features between 3200 and 3365 cm^{-1} are attributed to the quaternary ammonium. HPLC-ICP: chromatographic analysis showed coeluting peaks for tantalum and silicon. Viscosity (at 37 °C): 20 cps at 275 mg Ta/mL. Osmolality: 290 mOsm/kg at 275 mg Ta/mL. Zeta potential: −1.5 mV at neutral pH in a 15 mM NaCl and 2 mM $CaCl_2$ solution.

Characterization Methods. ICP−AES analyses were performed using a Perkin-Elmer 5300DV instrument equipped with a ryton Scott-type spray chamber, cross-flow nebulizer, quartz torch, and an alumina injector. The hydrodynamic sizes of the particles were measured by dynamic light scattering (DLS) at 25 °C using a Brookhaven Instruments Corporation Zeta PALS particle size analyzer. Conductivity was measured using a Traceable portable conductivity meter with a probe range up to 200 000 μS. ^{29}Si NMR spectra were obtained on a Varian INOVA 600 MHz spectrometer, and ^{1}H NMR spectra were collected on a 400 MHz Varian spectrometer. FT-IR spectra were recorded with 16 scans and a resolution of 4 cm^{-1} using an Avatar 370 by Thermo-Nicolet. Chromatographic analysis was achieved using an Agilent 1100 Series HPLC system equipped with an 1100 Series photodiode array detector in-line to a Varian Liberty II Radial inductively coupled plasma atomic emission spectrometer (ICP−AES). Separation was carried out using a Cadenza CW C18 (2 × 50 mm) reverse-phase column consisting of 3 μm particle media. Flow-injection analyses were performed using an Agilent 1100 Series HPLC system equipped with an 1100 Series photodiode array detector in-line to an AB Sciex QStar Elite quadruple time-of-flight (ToF) electrospray ionization (ESI) mass spectrometer. Viscosity measurements were carried out using an Anton Paar AMVn capillary viscometer. Osmolality measurements were performed using a VAPRO model 5520 vapor-point depression osmometer from Wescor, Inc., Biomedical Division. Zeta potential measurements were recorded using a Brookhaven Instruments Corporation (BIC) ZetaPALS with standard BIC issued electrodes. Multiple batches of ZMS-TaO were analyzed in aqueous pH-buffered solutions for reproducibility.

Agent Formulation. Concentrated phosphate-buffered saline (10× PBS) was added to 150 mg Ta/mL stock solution of ZMS-TaO until the agent solution reached osmolality of 290 mOsm/kg. The agent was tested for sterility using an EndoSafe unit after dilution to 0.3 mg Ta/mL to avoid interference observed above 1.5 mg Ta/mL. Sensitivity was limited to >5 EU/mL.

***In Vivo* Studies.** All tolerability and tissue retention studies were performed in male Lewis rats (weight range, 150−200 g). Formulated agents were injected *via* tail vein into awake and restrained rats ($n = 4$ per cohort). Bleeds were performed before injection, then 4 h, 1 day, 2 days, and 7 days after injection from tail vein catheter. Complete blood counts and clinical chemistry analysis were performed on these samples per previously published methods.[2] At indicated time points, injected rats were euthanized and necropsy was performed to collect organs. Tissues were analyzed per previously published methods.[2] Briefly, representative ~0.5 g sections of tissue were collected for microwave digestion and subsequent ICP−OES analysis. Samples were transferred quantitatively from VWR metal-free, sterile, polypropylene 50 mL centrifuge tubes into precleaned 100 mL CEM Corp XP-1500 Plus TFM fluoropolymer microwave vessel liners. Tubes were effectively rinsed of residual sample by sequentially adding solvent, vortex agitation, and transfer of 2 mL of 18 MΩ deionized water (DIW; Millipore, Bedford, MA, USA), 500 μL HF (46.0−51.0%) + 1 mL HNO_3 (70%) Ultrex II ultrapure reagent grade, and 2 mL of H_2O_2 (30−32%) "Baker Analyzed" ACS reagent grade (J.T. Baker, Phillipsburg, NJ, USA). Samples were allowed to predigest prior to sealing the microwave vessel assembly and processing in a MARSXpress (CEM Corp, Matthews, NC, USA) unit ramped to 180 °C in 15 min and held for 30 min. Vessels were allowed to cool to room temperature prior to depressurization and transfer to preweighed 50 mL centrifuge tubes containing 2 mL of 10 ppm Sc + 40 ppm of Zr in 1% HNO_3 as internal standard. Samples were brought to 20 mL total volume using 18 MΩ DIW and rinsing the microwave vessel a minimum of 3 times. Samples were then weighed.

To perform analysis, three replicates were collected with spectral conditions of 3 points per peak using 2-point background correction and source equilibration delay of 30 s. Matrix-matched standards in 5% HNO_3 + 0.5% HF of 0.2 to 100 ppm from Specpure 10,000 μg/mL $TaCl_5$ in 2% HF (Alfa Aesar, Ward Hill, MA, USA) stock were used for calibration and 1 ppm SPEX CertiPrep Multielement Solution 4 from stock 10 mg/L (Metuchen, NJ, USA) for quality control. ICP-OES rinse solution of 5% HNO_3 + 0.5% HF was pumped at flow rate 2.0 $mLmin^{-1}$ for 45 s between each analysis. Data was plotted as percent of injected dose (Ta) per organ.

Conflict of Interest: The authors declare no competing financial interest.

Acknowledgment. The authors would like to acknowledge the excellent technical assistance of A. M. Kulkarni, C. T. Zhang, T. A. Early, J. Crowder, D. deMoulpied, and J. Roberts along with the support of the Nanotechnology Advanced Technology Program at GE Global Research Center led by M. Blohm. P. Bonitatibus dedicates his contribution to the memory of his father.

Supporting Information Available: Analytical methods for physical characterization studies, additional figures (^{29}Si NMR, IR, ToF-MS, zeta potential, osmolality data, tissue retention plots, TEM, and DLS data), and tables (histopathology, clinical chemistry, and complete blood count data). This material is available free of charge *via* the Internet at http://pubs.acs.org.

REFERENCES AND NOTES

1. Yu, S.-B.; Watson, A. D. Metal-Based X-ray Contrast Media. *Chem. Rev.* **1999**, *99*, 2353–2377.
2. Torres, A. S.; Bonitatibus, P. J.; Colborn, R. E.; Goddard, G. D.; FitzGerald, P. F.; Lee, B. D.; Marino, M. E. Biological Performance of a Size-Fractionated Core−Shell Tantalum Oxide Nanoparticle X-ray Contrast Agent. *Invest. Radiol.* **2012**, in press.
3. Neun, B. W.; Stern, S. T. Monitoring Lysosomal Activity in Nanoparticle-Treated Cells. *Methods Mol. Biol.* **2011**, *697*, 207–212.
4. Johnson-Lyles, D. N.; Peifley, K.; Lockett, S.; Neun, B. W.; Hansen, M.; Clogston, J.; Stern, S. T.; McNeil, S. E. Fullerenol Cytotoxicity in Kidney Cells is Associated with Cytoskeleton Disruption, Autophagic Vacuole Accumulation, and Mitochondrial Dysfunction. *Toxicol. Appl. Pharmacol.* **2010**, *248*, 249–258.
5. Stern, S. T.; Johnson, D. N. Role for Nanomaterial−Autophagy Interaction in Neurodegenerative Disease. *Autophagy* **2008**, *4*, 1097–1100.
6. Bonitatebus, P. J.; Colborn, R. E.; Kulkarni, A. M.; Torres, A. S.; Bales, B. C.; Axelsson, O. A. Nanoparticle-Based Imaging Agents for X-ray/Computed Tomography and Methods for Making Same. United States Patent Application 20070122620.
7. Bonitatibus, P. J.; Butts, M. D.; Colborn, R. E.; Kulkarni, A. M.; Hay, B. A.; Torres, A. S.; Bales, B. C.; Marino, M. E. Nanoparticle Contrast Agents for Diagnostic Imaging. United States Patent Applications 20100278734, 20100278748, and 20100278749.
8. Liu, X.; Huang, H.; Jin, Q.; Ji, J. Mixed Charged Zwitterionic Self-Assembled Monolayers as a Facile Way to Stabilize Large Gold Nanoparticles. *Langmuir* **2011**, *27*, 5242–5251.
9. Jin, Q.; Xu, J.-P.; Ji, J.; Shen, J.-C. Zwitterionic Phosphorylcholine as a Better Ligand for Stabilizing Large Biocompatible Gold Nanoparticles. *Chem. Commun.* **2008**, 3058–3060.
10. Kim, C. K.; Ghosh, P.; Pagliuca, C.; Zhu, Z.-J.; Menichetti, S.; Rotello, V. M. Entrapment of Hydrophobic Drugs in Nanoparticle Monolayers with Efficient Release into Cancer Cells. *J. Am. Chem. Soc.* **2009**, *131*, 1360–1361.
11. Agasti, S. S.; Chompoosor, A.; You, C.-C.; Ghosh, P.; Kim, C.-K.; Rotello, V. M. Photoregulated Release of Caged Anticancer Drugs from Gold Nanoparticles. *J. Am. Chem. Soc.* **2009**, *131*, 5728–5729.

12. Rouhana, L. L.; Jaber, J. A.; Schlenoff, J. B. Aggregation-Resistant Water-Soluble Gold Nanoparticles. *Langmuir* **2007**, *23*, 12799–12801.
13. Tatumi, R.; Fujihara, H. Remarkably Stable Gold Nanoparticles Functionalized with a Zwitterionic Liquid Based on Imidazolium Sulfonate in a High Concentration of Aqueous Electrolyte and Ionic Liquid. *Chem. Commun.* **2005**, 83–85.
14. Liu, W.; Choi, H. S.; Zimmer, J. P.; Tanaka, E.; Frangioni, J. V.; Bawendi, M. Compact Cysteine-Coated CdSe(ZnCdS) Quantum Dots for *in Vivo* Applications. *J. Am. Chem. Soc.* **2007**, *129*, 14530–14531.
15. Muro, E.; Pons, T.; Lequeux, N.; Fragola, A.; Sanson, N.; Lenkei, Z.; Dubertret, B. Small and Stable Sulfobetaine Zwitterionic Quantum Dots for Functional Live-Cell Imaging. *J. Am. Chem. Soc.* **2010**, *132*, 4556–4557.
16. Breus, V. V.; Heyes, C. D.; Tron, K.; Nienhaus, G. U. Zwitterionic Biocompatible Quantum Dots for Wide pH Stability and Weak Nonspecific Binding to Cells. *ACS Nano* **2009**, *3*, 2573–2580.
17. Susumu, K.; Oh, E.; Delehanty, J. B.; Blanco-Canosa, J. B.; Johnson, B. J.; Jain, V.; Hervey, W. J., IV; Algar, W. R.; Boeneman, K.; Dawson, P. E.; Medintz, I. L. Multifunctional Compact Zwitterionic Ligands for Preparing Robust Biocompatible Semiconductor Quantum Dots and Gold Nanoparticles. *J. Am. Chem. Soc.* **2011**, *133*, 9480–9496.
18. Chung, Y.-C.; Chen, I.-H.; Chen, C.-J. The Surface Modification of Silver Nanoparticles by Phosphoryl Disulfides for Improved Biocompatibility and Intracellular Uptake. *Biomaterials* **2008**, *29*, 1807–1816.
19. Jin, Q.; Liu, X. S.; Xu, J.-P.; Ji, J.; Shen, J.-C. Zwitterionic Phosphorylcholine-Protected Water-Soluble Ag Nanoparticles. *Sci. China Ser. B* **2009**, *52*, 64–68.
20. Jia, G.; Cao, Z.; Xue, H.; Xu, Y.; Jiang, S. Novel Zwitterionic-Polymer-Coated Silica Nanoparticles. *Langmuir* **2009**, *25*, 3196–3199.
21. Estephan, Z. G.; Jaber, J. A.; Schlenoff, J. B. Zwitterion-Stabilized Silica Nanoparticles: Toward Nonstick Nano. *Langmuir* **2010**, *26*, 16884–16889.
22. Rosen, J. E.; Gu, F. Surface Functionalization of Silica Nanoparticles with Cysteine: A Low-Fouling Zwitterionic Surface. *Langmuir* **2011**, *27*, 10507–10513.
23. Bonitatibus, P. J.; Torres, A. S.; Goddard, G. D.; FitzGerald, P. F.; Kulkarni, A. M. Synthesis, Characterization, and Computed Tomography Imaging of a Tantalum Oxide Nanoparticle Imaging Agent. *Chem. Commun.* **2010**, *46*, 8956–8958.
24. Nacken, M.; Hoebbel, D.; Schmidt, H. Formation and Hydrolytic Stabilty of Oxygen Bridged Heterometal Bonds (Si-O-Ti, Si-O-Zr, Si-O-Ta) in Sol-Gel Materials. *Mater. Res. Soc. Symp. Proc.* **1991**, *576*, 221–226.
25. Schulz, H.; Pratsinis, S. E.; Ruegger, H.; Zimmermann, J.; Klapdohr, S.; Salz, U. Surface Functionalization of Radiopaque Ta_2O_5/SiO_2. *Colloids Surf. A* **2008**, *315*, 79–88.
26. Eloy, R.; Corot, C.; Belleville, J. Contrast Media for Angiography: Physicochemical Properties, Pharmacokinetics and Biocompatibility. *Clin. Mater.* **1991**, *7*, 89–197.
27. Jakobsen, J. A. Physiological Effects of Contrast Media for Use in Multidetector Row Computed Tomography. *Eur. J. Radiol.* **2007**, *62*, 14–25.
28. Roth, R.; Akin, M.; Deligonul, U.; Kern, M. J. Influence of Radiographic Contrast Media Viscosity to Flow through Coronary Angiographic Catheters. *Cathet. Cardiovasc. Diagn.* **1991**, *22*, 290–294.
29. Neun, B. W.; Dobrovolskaia, M. A. Detection and Quantitative Evaluation of Endotoxin Contamination in Nanoparticle Formulations by LAL-based Assays. *Methods Mol. Biol.* **2011**, *697*, 121–130.
30. Dobrovolskaia, M. A.; Neun, B. W.; Clogston, J. D.; Ding, H.; Ljubimova, J.; McNeil, S. E. Ambiguities in Applying Traditional Limulus Amebocyte Lysate Tests To Quantify Endotoxin in Nanoparticle Formulations. *Nanomedicine* **2010**, *5*, 555–562.
31. McIntire, G. L.; Bacon, E. R.; Illig, K. J.; Coffey, S. B.; Singh, B.; Bessin, G.; Shore, M. T.; Wolf, G. L. Time Course of Nodal Enhancement with CT X-ray Nanoparticle Contrast Agents: Effect of Particle Size and Chemical Structure. *Invest. Radiol.* **2000**, *35*, 91–96.
32. Estephan, Z. G.; Schlenoff, P. S.; Schlenoff, J. B. Zwitteration as an Alternative to PEGylation. *Langmuir* **2011**, *27*, 6794–6800.
33. Starck, P.; Mosse, W. K. J.; Nicholas, N. J.; Spiniello, M; Tyrrell, J.; Nelson, A.; Qiao, G. G.; Ducker, W. A. Surface Chemistry and Rheology of Polysulfobetaine-Coated Silica. *Langmuir* **2007**, *23*, 7587–7593.
34. Zhou, W.; Shao, J.; Jin, Q.; Wei, Q.; Tang, J.; Ji, J. Zwitterionic Phosphorylcholine as a Better Ligand for Gold Nanorods Cell Uptake and Selective Photothermal Ablation of Cancer Cells. *Chem. Commun.* **2010**, *46*, 1479–1481.
35. Matsuura, K.; Ohno, K.; Kagaya, S.; Kitano, H. Carboxybetaine Polymer-Protected Gold Nanoparticles: High Dispersion Stability and Resistance Against Non-specific Adsorption of Proteins. *Macromol. Chem. Phys.* **2007**, *208*, 862–873.
36. Akiyama, T.; Ibata, C.; Fujihara, H. Water Soluble Palladium and Gold Nanoparticles Functionalized by a New Phosphine with Zwitterionic Liquid Based on Imidazolium Sulfonate Linked Ethylene Glycol Moiety. *Heterocycles* **2010**, *80*, 925–931.
37. Choi, H. S.; Liu, W.; Liu, F.; Nasr, K.; Misra, P.; Bawendi, M. G.; Frangioni, J. V. Design Considerations for Tumour-Targeted Nanoparticles. *Nat. Nanotechnol.* **2010**, *5*, 42–47.
38. Choi, H. S.; Liu, W.; Misra, P.; Tanaka, E.; Zimmer, J. P.; Ipe, B. I.; Bawendi, M. G.; Frangioni, J. V. Renal Clearance of Quantum Dots. *Nat. Biotechnol.* **2007**, *25*, 1165–1170.
39. Wistrand, L. G.; Rogstad, A.; Hagelin, G.; Roed, L.; Oulie, I.; Gram, A.; Evans, P.; Rasmussen, H.; Grant, D.; Iveson, P.; *et al.* GE-145, A New Low-Osmolar Dimeric Radiographic Contrast Medium. *Acta Radiol.* **2010**, *51*, 1014–1020.
40. Flondor, M.; Hofstetter, C.; Boost, K. A.; Betz, C.; Homann, M.; Zwissler, B. Isoflurane Inhalation after Induction of Endotoxemia in Rats Attenuates the Systemic Cytokine Response. *Eur. Surg. Res.* **2008**, *40*, 1–6.
41. Neun, B. W.; Dobrovolskaia, M. A. Qualitative Analysis of Total Complement Activation by Nanoparticles. *Methods Mol. Biol.* **2011**, *697*, 237–245.
42. Zolnik, B. S.; González-Fernández, Á.; Sadrieh, N.; Dobrovolskaia, M. A. Nanoparticles and the Immune System. *Endocrinology* **2010**, *151*, 458–465.
43. Dobrovolskaia, M. A.; Germolec, D. R.; Weaver, J. L. Evaluation of Nanoparticle Immunotoxicity. *Nature Nanotechnol.* **2009**, *4*, 411–414.